Hypersonic acoustic excitations in binary colloidal crystals: Big versus small hard sphere control

G. Tommaseo
Max Planck Institute for Polymer Research, P.O. Box 3148, 55021 Mainz, Germany

G. Petekidis
Department of Materials Science and Technology, University of Crete and FORTH, P.O. Box 1527, GR-71110 Heraklion, Greece

W. Steffen
Max Planck Institute for Polymer Research, P.O. Box 3148, 55021 Mainz, Germany

G. Fytas
Max Planck Institute for Polymer Research, P.O. Box 3148, 55021 Mainz, Germany and Department of Materials Science and Technology, University of Crete and FORTH, P.O. Box 1527, GR-71110 Heraklion, Greece

A. B. Schofield
School of Physics and Astronomy, University of Edinburgh, Edinburgh EH9 3JZ, United Kingdom

N. Stefanou
Department of Solid State Physics, University of Athens, Panepistimioupolis, GR-15784 Athens, Greece

(Received 8 September 2006; accepted 4 December 2006; published online 4 January 2007)

The phononic band structure of two binary colloidal crystals, at hypersonic frequencies, is studied by means of Brillouin light scattering and analyzed in conjunction with corresponding dispersion diagrams of the single colloidal crystals of the constituent particles. Besides the acoustic band of the average medium, the authors' results show the existence of narrow bands originating from resonant multipole modes of the individual particles as well as Bragg-type modes due to the (short-range) periodicity. Strong interaction, leading to the occurrence of hybridization gaps, is observed between the acoustic band and the band of quadrupole modes of the particles that occupy the largest fractional volume of the mixed crystal; the effective radius is either that of the large (in the symmetric NaCl-type crystalline phase) or the small (in the asymmetric $NaZn_{13}$-type crystalline phase) particles. The possibility to reveal a universal behavior of the phononic band structure for different single and binary colloidal crystalline suspensions, by representing in the dispersion diagrams reduced quantities using an appropriate length scale, is discussed. © *2007 American Institute of Physics*. [DOI: 10.1063/1.2429067]

I. INTRODUCTION

Colloidal systems consist of mesoscopic particles dispersed in a continuous medium, and it is basically the particle size that distinguishes these systems from other materials, such as solutions. The hallmark of colloids is their ability to crystallize like atomic systems and, for hard sphere interactions, the one-dimensional phase diagram depends only on their volume fraction.[1] The characteristic lattice spacing of these structures falls into the submicron range and, therefore, colloidal crystals are able to mold the flow of light (photonic crystals)[2] and sound at hypersonic frequencies.[3] The propagation of phonons with wavelengths commensurate with the spacing of the colloidal crystals, i.e., with optical wavelengths and hence at hypersonic (gigahertz) frequencies, can be uniquely studied by (inelastic) Brillouin light scattering (BLS) at a selected scattering wave vector $\mathbf{q}=\mathbf{k}_i-\mathbf{k}_s$, where $\mathbf{k}_i$ and $\mathbf{k}_s$ are the wave vectors of the incoming and outgoing photons.[4–7] This nondestructive and noncontact high-resolution technique is based on the scattering of single frequency laser light by the phonons with wave vector $\mathbf{k}$ propagating in the medium at thermal equilibrium. For homogeneous media over the length scale $\sim q^{-1}$, $\mathbf{q}=\mathbf{k}$, i.e., $\mathbf{q}$ matches $\mathbf{k}$ of the selected phonon with a longitudinal or transverse phase velocity c. In this case, the spectrum $I(q,\omega)$ displays one Brillouin doublet at $\omega=\pm cq$ on both sides of the elastic (at $\omega=0$) central Rayleigh line. For inhomogeneous media exceeding the length q^{-1}, additional acoustic excitations are, in principle, expected.

In colloidal crystals, as requested by the translation symmetry of the lattice, phonons with wave vectors $\mathbf{k}$ and $\mathbf{k}+\mathbf{G}$, with $\mathbf{G}$ being a vector of the reciprocal lattice, represent the same wave field. This leads to a description of the frequency levels of a phonon in a colloidal crystal in terms of a family of continuous functions $\omega_n(\mathbf{k})$, $n=1,2,\ldots$, each with the periodicity of the reciprocal lattice. The information contained in these functions is referred to as the phononic band structure of the colloidal crystal, by analogy to the energy band structure associated with the electron states in ordinary crystalline solids.[8] It turns out that there are regions of frequency, so-called phononic band gaps, where no propagating

phonon modes exist in a colloidal crystal. Such gaps open up, for example, when two phonon dispersion lines (phononic bands) of the same symmetry cross each other, about the crossing point, as a result of level repulsion due to the mutual interaction. This is the case of Bragg gaps at the Brillouin zone (BZ) boundaries where acoustic bands, originating from different points of the reciprocal lattice, cross each other. The same mechanism also operates when bands of different physical origins are involved (hybridization gaps), e.g., an extended acoustic band and a narrow band formed from interacting resonant modes of the individual particles.

The phonon spectrum of crystalline suspensions of colloidal particles with radius R in the range of 120–400 nm recorded by BLS using tandem Fabry-Pérot interferometry in the gigahertz frequency region has revealed three characteristic groups of elastic excitations: opticlike modes reflecting vibration modes of the individual particles,[4,6,7,9,10] mixed hybrid modes between acoustic phonons of the average medium and particle modes, and Bragg-type modes due to some crystalline or short-range order.[7,11,12] Although an adequate overall theoretical description of the experimental rich dispersion relations was achieved, clear signatures from the particle (geometrical and mechanical properties) and the structure were not identifiable. In fabricated latex spheres opals,[10] a rich spectrum of multipole particle resonances (up to 21) were identified by their angular-momentum index l. In the colloidal suspensions, the lowest particle modes, corresponding to $l=2$, seem to be relevant for the observed weak hybridization gap.[4,6,12] However, Bragg gaps at the BZ boundaries are also expected in the same region of the dispersion plot. For the Bragg-type modes, which comply with the condition $\mathbf{q}=\mathbf{k}+\mathbf{G}$, a direct relation to the lattice spacing is missing. Clearly, a fundamental understanding of the interplay between the various elastic excitations and the crystal structure of the composite medium is essential.[13] Experimentally, binary colloidal mixtures offer the opportunity for an independent variation of the size of the unit cell and the particle dimensions. The former determines the frequency position of the Bragg gaps, while the latter control the particle eigenfrequencies.[3,14–16]

Binary mixtures of monodisperse hard sphere colloids may self-assemble to form binary crystals similar to those encountered in atomic systems. Such superlattice structures were identified experimentally both in natural gem opals[17] as well as in synthetic ones of sterically stabilized particles.[18] The symmetry of the crystal phase critically depends on the volume fraction and size ratio of the two spheres denoted by S and L (or M).[18] For example, the equimolar LS colloidal crystal may form a face-centered-cubic (fcc) NaCl-type crystalline phase, whereas the asymmetric mixture MS_{13} may crystallize in the cubic $NaZn_{13}$ structure. In these systems, the lattice spacing can significantly deviate from the diameters of the individual particles, and hence a comparison of the phonon propagation in binary and single colloidal crystals will be crucial for the assessment of the particle and structure fingerprints in the dispersion relations. In the case of the LS crystalline phase, the large spheres (L) control the spacing, whereas in the superlattice structure of MS_{13}, the lattice spacing is much larger than that in both M and S individual crystals. Furthermore, the prediction of the static and dynamic properties of binary colloidal crystals on the ground of the component crystalline phases is of general interest not only in materials science. Some properties, e.g., density, remain unchanged, whereas some others, e.g., elastic excitations, witness strong modification.

II. EXPERIMENT

A. Setup

A solid state neodymium-doped yttrium aluminum garnet laser with continuous wave propagation ($\lambda=532$ nm) was mounted perpendicularly to the x-y plane on the edge of a goniometer.[7] A small part of the laser beam is split and guided through a fiber into the Fabry-Pérot interferometer. This reference beam assures a stabilization of the interferometer without loss of the sensitivity needed for long time measurements. Due to optical components (such as prisms, Glan polarizer, and mirrors) necessary to guide the laser beam through the center of a goniometer and to insure complete vertically polarized light with respect to the scattering plane, the laser impinges on the sample with a power of about 60 mW. The scattered light is focused, after passing from a Glan-Thomson polarizer to select its vertically polarized component, through a lens onto the pinhole aperture ($\varnothing=200\ \mu$m) of a six-pass tandem Fabry-Pérot interferometer (TFPI). A synchronized mechanical shutter placed in front of the entrance of the interferometer cuts out the Rayleigh peak, which originates from elastic scattering, when the TFPI piezoelectrically scans through the frequency of the incident light. By rotating the arm of the goniometer we can change the scattering angle θ without moving around the complete TFPI setup. Because of setup limitations, the scattering angle ranges only from $\theta=6°$ to $\theta=150°$. An avalanche photodiode connected to a multichannel analyzer transfers the collected scattered light to a PC for further signal processing. The measured spectra presented in the next section were taken at different free spectral ranges (6, 7.5, 15, 20, and 30 GHz) so that both high resolution and broad frequency range for the different systems investigated could be assured.

B. Systems

Two binary mixtures of colloidal systems, with different dimensions of their single component colloids, were investigated. The hard spheres used in both binary systems consist of poly (methylmethacrylate) (PMMA) particles, which are sterically stabilized by a thin layer of poly-12-hydroxystearic acid about 10 nm thick. The elastic constants of PMMA and the stabilizing layer are different mainly because of interpenetration of solvent in the thin layer, so the latter should have elastic constants between those of PMMA and the solvent. But these cannot be easily evaluated. However, the layer is thin and thus we may assume that the particles are homogeneous with the elastic properties of PMMA.[7] The colloids were then dispersed in a solvent mixture consisting of 70% *cis*-decalin and 30% tetralin, in order to achieve a better refractive index matching and thus eliminate multiple scattering.

Colloidal hard sphere suspensions are known to exhibit a liquid to crystal transition, due to entropic reasons only, at a volume fraction of 0.494.[1] Up to a volume fraction of 0.545 the system is in a liquid-crystal coexistence with the dense crystal phase (0.545) occupying the bottom part of the vial and the liquid phase (0.494) the top part due to an overall density mismatch. The phase separation normally lasts a few to several hours, after preparation of the sample, depending on the particle polydispersity. At volume fractions higher than 0.545 the system is fully crystalline; although above around 0.58, the system is kinetically trapped in a metastable glassy state.[1] Binary mixtures of hard spheres, on the other hand, may form a variety of complicated crystal structures depending on the total colloid volume fraction, the particle size ratio, and the stoichiometry.[1,18] Similar to their single-particle counterparts they need several hours, or more, to phase separate, and the two phases separate due to gravity with the crystal phase at the bottom. Thus, the volume fraction and type of crystal structure are predetermined by the total colloid volume fraction and stoichiometry of the specific sample (with certain size ratio).

The first binary system examined is a NaCl (fcc) crystal, which has a stoichiometry of LS. This consists of large (L) particles with a radius of 344 nm arranged in a fcc lattice containing small particles (S) with a radius of 140 nm in the octahedral interstitial holes, as shown in the model in Fig. 1(a). Laser light crystallography was used to determine the lattice parameter a as 1006 nm. This corresponds to volume-filling fractions 0.670 and 0.045, for the L and S particles, respectively, resulting in a total volume-filling fraction $\phi = 0.715$. However, to make absolutely sure that the sample has the required LS stoichiometry (and was not, say, fcc LS_2 or even just a crystal of pure L, both of which could give a very similar crystallographic scattering trace to that of fcc LS), scanning electron microscopy (SEM) pictures of the crystal were also taken. This involved drying down some of the samples under ambient conditions and sticking the resultant white powder on a microscope stub and sputter-coating it with a very thin layer of gold to make it conductive to the imaging electrons. The sample was then examined using a Cambridge S250 SEM. Pictures collected this way are shown in Figs. 1(b) and 1(c), and, when compared with the fcc LS model next to them, both the square (001) and the hexagonal (111) planes of the structure can be seen in the colloidal crystal.

The second binary system examined is a MS_{13} superlattice structure made up of large (M) particles with a radius of 241 nm and small (S) particles with a radius of 140 nm. In this structure the large spheres form a cube inside of which sit 13 small spheres, arranged at the 12 vertices and the center of an icosahedron. The icosahedra of neighboring cubes are rotated by 90° with respect to each other to give a superlattice structure made up of eight simple cubic subcells, as shown in the inset of Fig. 1(d). For the sample under investigation, laser light crystallography[18] was used to confirm the exact structure present and determine the crystal lattice constant. This is shown in Fig. 1(d). The peaks are indexed using Miller indices with the usual simple cubic parameters being doubled because the lattice constant of the primitive cell is twice the edge of the cubic subcell. The presence of the (531) line confirms that the structure seen is the superlattice MS_{13} and from the position of the other peaks the lattice constant a is calculated to be 1420 nm. From the above values of the particle radii and the lattice constant, the volume-filling fractions of the M and S particles are calculated to be 0.164 and 0.418, respectively, resulting in a total volume-filling fraction $\phi = 0.582$.

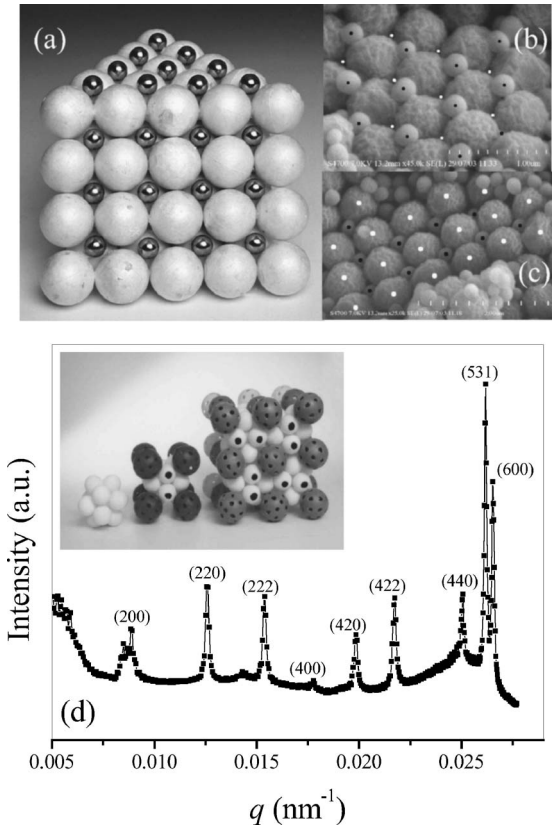

FIG. 1. (a) A model of the LS fcc binary crystal. (b) The (111) plane of the binary fcc LS crystal from the actual sample. The black spots show the position of the small spheres within this plane, while the white spots show the gaps between them in which sit the large spheres from the layer above. (c) The (001) plane of the actual fcc LS crystal with the white spots showing the square arrangement of the large L spheres and the black spots the small S spheres sat between them. (d) The laser light scattering trace of the MS_{13} binary crystal (here, q denotes the magnitude of the difference between the wave vectors of the diffracted and the incident light beams). The inset shows models of the central icosohedal packing of the 13 small spheres, a cubic subunit made up of a cube of large M spheres and the orientation of the icosahedron within it, and the full superlattice structure showing the 90° rotation of the icosohedra between neighboring subunits.

The lattice constant of the single colloidal crystals S, M, and L was deduced from the relation $a/R = (16\pi/3\phi)^{1/3}$ which holds for fcc crystals, at the given volume-filling fraction $\phi = 0.545$. The geometrical characteristics of the different crystals are given in Table I. The elastic properties of the colloid particles and the solvent mixture are determined[7,12] by the longitudinal and transverse sound velocities in PMMA, $c_{pt} = 1400$ m/s and $c_{pl} = 2700$ m/s respectively, as well as the (longitudinal) sound velocity $c = 1500$ m/s in the pure solvent. The densities used for the particle and solvent were the literature values of $\rho_p = 1180$ kg/m^3 and $\rho = 926$ kg/m^3, respectively.

TABLE I. Characteristic dimensions of the crystalline colloidal (PMMA) suspensions.

Sample	R (nm)	a (nm)	a/R	ϕ
S	140	438.6	3.133	0.545
M	241	755	3.133	0.545
L	344	1077.6	3.133	0.545
LS	344/140	1006	2.924/7.186	0.670/0.045
MS_{13}	241/140	1420	5.892/10.143	0.174/0.418

III. RESULTS

A. Brillouin light scattering spectra

Typical experimental BLS spectra of the crystalline symmetric binary LS colloidal suspensions at low and high scattering wave vector **q** recorded at two free spectral ranges (7.5 and 30 GHz) are shown in Fig. 2 along with the spectra of the single colloidal suspensions of the constituent particles, L and S, for comparison. The BLS spectra were represented by a superposition of up to five Lorentzian line shapes convoluted with instrumental function. Each Lorentzian line is characterized by three parameters: the amplitude A_i, the peak position f_i $(=\omega_i/2\pi)$, and the half-width at half maximum Γ_i. For example, the individual Lorentzian components in the total BLS spectrum of L are shown in the lower panel of Fig. 2. The central region of the spectrum about ±1 GHz around the Rayleigh line is kept for the reference beam used for the stabilization of the interferometer and is hence omitted in the plots of the experimental spectra of Figs. 2–4. An inspection of the spectra of Fig. 2 reveals closer similarity between LS and L than between the LS and S systems.

Figure 3 shows representative BLS spectra of the asymmetric binary crystalline colloidal suspension MS_{13} along with the spectra of the constituent M and S colloidal crystals recorded at 6 and 15 GHz at low and high q, respectively. Their representation by superposition of Lorentzian line shapes convoluted with the instrumental function is shown in the case of the M system as an example. Both Figs. 2 and 3 indicate that the BLS line shapes become quite rich as the spatial resolution increases with q. This already occurs in the first BZ, as depicted in the two panels of Fig. 4, which display BLS spectra of LS and MS_{13} at different q values. While at the lowest q the asymmetric MS_{13} exhibits only a

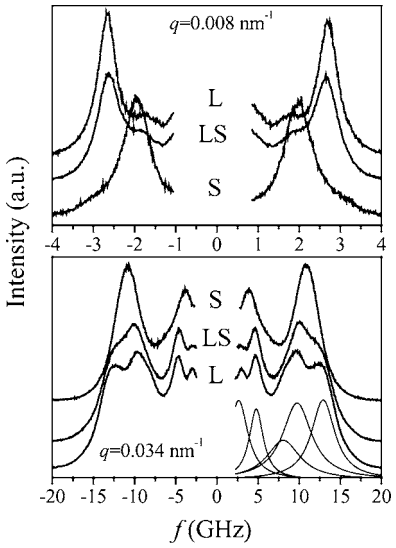

FIG. 2. Experimental BLS spectra of the symmetric binary LS, and the single L and S component crystals recorded at two different values of the wave number using different free spectral ranges (7.5 GHz in the upper panel and 30 GHz in the lower panel) to achieve optimal resolution. The central region of the spectrum used for the reference beam to stabilize the interferometer is omitted for clarity reasons. A representative fitting of the experimental spectra by superposition of Lorentzian line shapes convoluted with the instrumental function is shown in the case of the L system by displaying the five necessary contributions (lower panel).

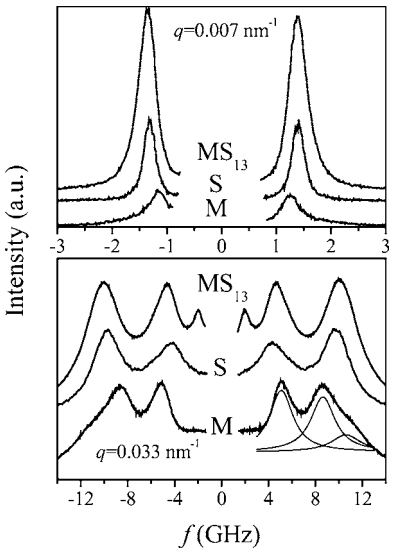

FIG. 3. Experimental BLS spectra of the asymmetric binary MS_{13}, and the single M and S component crystals recorded at two different values of the wave number using different free spectral ranges (6 GHz in the upper panel and 15 GHz in the lower panel). A representative fitting of the experimental spectra by superposition of Lorentzian line shapes convoluted with the instrumental function is shown in the case of the M system by displaying the three necessary contributions (lower panel). As in Fig. 2, the central region of the spectrum is omitted.

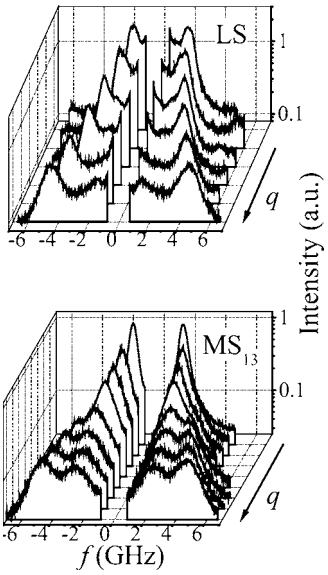

FIG. 4. The evolution of the BLS spectral features in the two binary colloidal mixtures with q; q varies from 0.003 to 0.011 nm^{-1} for LS and from 0.008 to 0.015 nm^{-1} for MS_{13}.

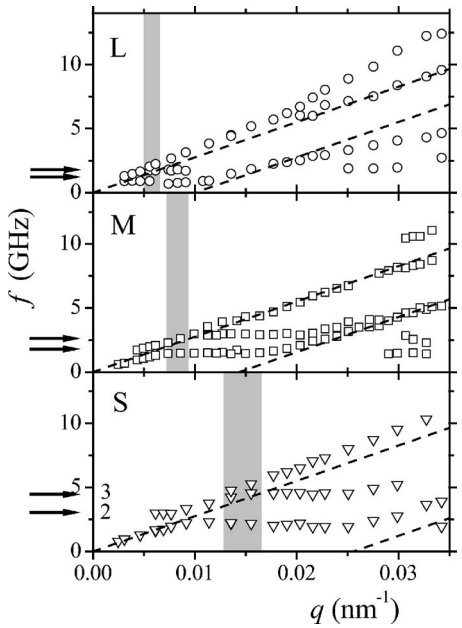

FIG. 5. Phonon dispersion relations of the single crystalline colloidal suspensions. The two lower particle eigenmodes, corresponding to $l=2$ and $l=3$, are indicated by the arrows on the frequency axis. The extension of the first BZ is marked, in each case, by the gray-shaded area. The dashed lines in each diagram show effective-medium dispersion curves originating from the central and from the first neighboring points of the reciprocal lattice (Bragg modes).

single doublet, as anticipated for a homogeneous effective medium in the low q limit, the symmetric LS displays more than one acoustic excitation and the evolution of the BLS with q is different. The character of the observed acoustic modes is reflected in the dispersion diagrams of the system.

B. Dispersion relations

The frequencies f_i $(i=1,2,\ldots)$ of the different modes in the three single colloidal crystals are plotted versus q in Fig. 5. The different modes are grouped in four types characterized by their dispersion and location in reciprocal space, i.e., q larger or smaller than G. These are (i) the long-wavelength acoustic phonon modes of the average medium $(qR \leqslant 1)$, (ii) flatbands originating from the interacting resonant 2^l-pole modes of the individual particles, identified by the corresponding angular-momentum index l, (iii) Bragg-type modes which are the fingerprints of the crystalline structure or short-range liquidlike order usually observed at high q/low f, and (iv) q-dependent modes in the $qR>1$ region. We note that the present colloidal suspensions are polycrystalline and, therefore, the direction of $\mathbf{q}$ in reciprocal space is not well defined. The extension of the boundaries of the first BZ of the three single colloidal suspensions is marked, in each panel of Fig. 5, by a gray-shaded area (the distance of the boundaries from the center of the fcc BZ varies between $\sqrt{3}\pi/a$ in the ΓL direction and $\sqrt{5}\pi/a$ in the ΓW direction). The two arrows in the f axis for each system indicate the eigenfrequencies of the $l=2,3$ lowest particle modes, as obtained from single-particle scattering calculations.[4,6,7,9–13]

The acoustic range of the average medium is restricted in the $qR \leqslant 1$ region, i.e., when the phonon wavelength exceeds $2\pi R$. The corresponding sound velocity amounts to 1650 ± 40 m/s, which is about 4% lower than the value deduced from the effective-medium theory.[19] However, since the hybridized bands are pushed down below the crossing point,[13] the sound velocity should be deduced from low-frequency (and hence low-q) data, well below the hybridization region, in order to avoid underestimation of its value. Since this cannot be always insured experimentally, we have used the theoretical effective sound velocity, $c_{\text{eff}}=1730$ m/s, for S, M, and L $(\phi=0.545)$ to draw the effective-medium dispersion lines in Fig. 5 (dashed lines). This is calculated from the equation:[19]

$$c_{\text{eff}} = c\left\{\frac{\rho_{\text{eff}}}{\rho}\left[1-\phi+\phi\frac{\rho}{\rho_p}\left[(c_{pl}/c)^2-\frac{4}{3}(c_{pt}/c)^2\right]^{-1}\right]\right\}^{-1/2},$$

where

$$\rho_{\text{eff}} = \rho\frac{1-\phi+(2+\phi)\rho_p/\rho}{1+2\phi+2(1-\phi)\rho_p/\rho}.$$

Similarly, for the effective sound velocities of LS $(\phi=0.715)$ and MS_{13} $(\phi=0.582)$, we use the corresponding theoretical values 1849 and 1753 m/s, respectively. The extended region of the pure acoustic behavior well beyond the first BZ in the different systems is remarkable.

The observed phononic gap is (as will be shown below) a hybridization gap; it results from the interaction of the lowest $(l=2)$ particle modes with the acoustic modes of the average medium.[13] In other words, this is not a Bragg gap[3,14–16] occurring at the boundaries of the first BZ as can be seen, e.g., in the dispersion diagram of the S colloidal crystalline suspension where the gap is clearly inside the BZ. Besides this gap, there is a splitting of the effective-medium band in the vicinity of the eigenfrequency of the $l=3$ particle mode in all three single colloidal crystals. For colloids of bigger spheres, there is a larger number of particle eigenmodes in the frequency region under consideration. Therefore the experimental points in the high-f region for the M and especially for the L systems that deviate from the dispersion line of the effective medium (dashed line starting from $q=0$) may belong to flatbands originating from higher-order particle modes. The most pertinent finding in the single colloidal crystals under consideration is the appearance of a clear phononic gap in the vicinity of the eigenfrequency of the lowest quadrupole particle mode.

The Bragg modes usually observed at high q/low f, which require crystalline structure or short-range liquidlike order, are also clearly visible. Particularly in the M system, the lattice constant of which allows a clear observation of two neighboring BZs within the accessible range of q values, the majority of the observed Bragg modes follow nicely an effective-medium dispersion line originating from the first neighboring reciprocal lattice point (lower dashed line). Hybridization with the relevant flatbands of particle modes is also discernible. Similar is the case of the S system. On the other hand, in the L system, though higher-order Bragg modes are also experimentally accessible, the formation of corresponding bands cannot be easily deduced from the data available.

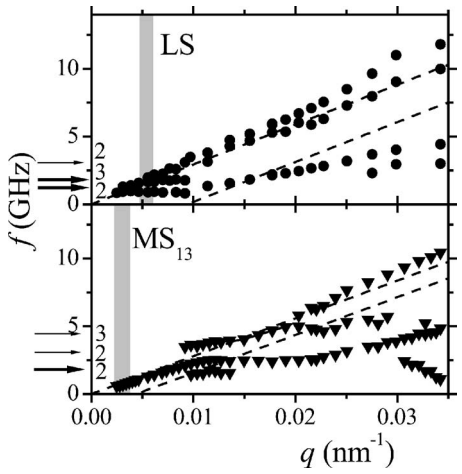

FIG. 6. Phonon dispersion diagrams of the binary colloidal crystals LS and MS_{13}. The notation is as in Fig. 5. The thick and the thin arrows indicate the eigenfrequencies of the modes of the large and the small particles, respectively.

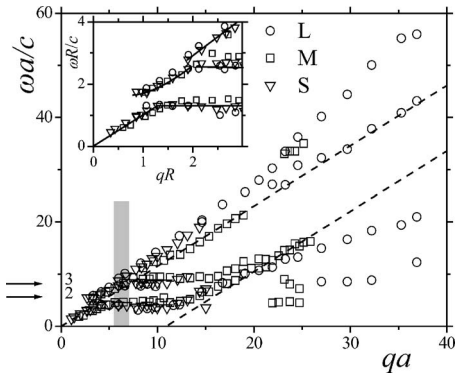

FIG. 7. A reduced phonon dispersion diagram for the three single colloidal crystals using the experimental points of Fig. 5, the relevant dimensions from Table I, and the (longitudinal) sound velocity c in the solvent. The notation is as in Fig. 5. Inset: A detailed view of the corresponding $\omega R/c$ vs qR dispersion diagram about the hybridization gaps, with R being the particle radius. The lines are guide to the eye.

In the mixtures, the presence of two spheres of different sizes, each sphere with a different volume-filling fraction, and the different crystalline structures (a symmetric NaCl structure and a superlattice MS_{13}) will have an impact on the phonon propagation, and the main objective of this study is to quantify the induced changes and possibly account for them. The ultimate goal is then to reliably predict the acoustic properties of the colloidal mixtures based on the geometric and/or structural characteristics of the constituent components. The two binary crystalline colloidal suspensions under consideration possess distinct similarities and disparities with the crystalline suspensions of the single constituent particles, as suggested by the ratio a/R in Table I.

The characteristic feature of the symmetric LS is the closeness of its lattice constant to that of the colloidal crystal of the large component, i.e., $a(\mathrm{LS}) \approx a(\mathrm{L})$. This system will allow us to distinguish and identify the main modes in the dispersion relations which selectively depend on one of the two lengths, a and R. According to the upper panel of Fig. 6, three particle eigenmodes are discernible in the LS binary mixture. From these, two modes of the large particles (those with $l=2,3$) are clearly resolved, whereas the presence of the ($l=2$) modes of the small particles is witnessed by the splitting of the effective-medium band. It is the flatband of quadrupole modes of the large particles with the lowest frequency which is found to determine the phononic gap in LS. The band of quadrupole modes of the small particles is responsible for the splitting of the effective-medium band at about 3 GHz. Overall, the phonon propagation in LS resembles that in L.

For the MS_{13} system, the characteristic feature is its large spacing which is distinctly different from the lattice parameter in the individual M and S crystalline components, i.e., $a(\mathrm{MS}_{13}) > a(\mathrm{M}) > a(\mathrm{S})$. In this case, the large disparity between a and R of the constituent particles (see Table I) will help us to assign the relevance of the morphological and particle characteristics on sound propagation in these hypersonic crystalline colloidal suspensions. Like in LS, three particle eigenmodes indicated by arrows in the lower panel of Fig. 6 are resolved. In this mixed crystal, however, the two higher eigenmodes ($l=2,3$) belong to the small particles, and the lowest quadrupole modes are associated with the large colloidal particles. The phononic gap is now determined by the band of quadrupole modes of the small *and not* of the large particles. In contrast to the LS system, no appreciable interaction is manifested between the flatband of quadrupole modes of the large particles and the acoustic band of the average medium. The extended region of the pure acoustic behavior well beyond the first BZ is remarkable. Overall, the behavior resembles that of the S component.

The phonon dispersion relations in the polycrystalline colloidal suspensions under consideration depend on both the size of the colloidal particles and their structural arrangement, which control the particle vibrations and the displacement field in the composite medium. In the case of the single colloidal crystals, at a given ϕ, the two length scales R and a are equivalent since $a=2.56R/\phi^{1/3}$, and the scaling[13] of the experimental dispersion curves applies for both lengths R and a. This equivalence, however, is removed in the mixed crystals progressively from LS to MS_{13} (Table I). We shall next examine the scaling concepts in the dispersion diagrams of the different colloidal crystals under consideration.

IV. DISCUSSION

A. Single colloidal crystals

A successful superposition of all observed modes in the three single colloidal crystals is obtained in the presentation $\omega a/c$ versus qa of Fig. 7 with no adjustable parameter. Other alternative plots, such as $\omega R/c$ versus qR, $\omega R/c$ versus qa, and $\omega a/c$ versus qR, would look alike since the ratio a/R is the same for the three systems; this of course does not apply for the binary crystals. The plot of Fig. 7 nicely demonstrates that the hybridization gap occurs in the vicinity of the eigenfrequency of the quadrupole particle modes.

According to the above, tuning of the gap is possible through the size of the particle, its elastic properties, and the volume-filling fraction in a given medium. Crystallinity is not a prerequisite for the existence of the hybridization gap, which occurs even in the disordered state ($\phi < 0.5$)[4,12] pro-

vided that the average distance between neighboring particles is within the decay length of the phonon. The latter $\sim c_{\mathrm{eff}}/\Gamma \sim 3-4$ μm (as estimated using an effective sound velocity $c_{\mathrm{eff}} \sim 1700$ m/s and a Brillouin linewidth $\Gamma \sim 0.5$ GHz) is of the order of the lattice constant due to the relatively short lifetime $(\sim 1/\Gamma)$ of the thermal phonons in liquids. For the smallest particle diameter, ϕ could be as low as 0.1. However, both the width of the gap[13] and the experimental signal decrease with dilution. This can be understood as follows. As ϕ decreases, the interaction between neighboring particles becomes weaker and the bands originating from the multipole modes of the interacting particles get narrow. The wave field associated with these band modes is strongly localized about the individual particles and the overlap with the acoustic field of the extended states in the (homogeneous) effective medium is reduced. Consequently, the hybridization between bands of particle modes and the effective-medium band becomes weaker, and the gaps that open up as a result of this hybridization narrow. On the other hand, the particle modes are more strongly localized as l increases, and this explains why only the gap corresponding to the lowest quadrupole particle mode is discernible.

The Bragg modes usually observed at high q/low f, which require a crystalline structure or a short-range liquidlike order, are superimposed in all three systems in the presentation of Fig. 7. Noncrystalline dense colloidal suspensions exhibit also high q/low f modes,[12] but their intensity is higher in the presence of crystalline order.[7] Most likely, Bragg-type modes emerge as soon as a liquidlike ordering is established in dense colloidal suspensions.

The experimental points in the high-f region that deviate from the effective-medium band are essentially obtained only in the L system and may belong to flatbands of higher-order particle modes. However, the distribution of these points is relatively sparse in order to unambiguously substantiate this interpretation.

B. LS (NaCl structure)

In the crystalline binary mixtures, there are two spheres of different sizes and a proper length scale should be chosen in order to construct a reduced dispersion diagram for the mixed crystal and its constituents. The characteristic feature of LS is the closeness of the lattice constants of the mixed crystal and the single crystal L of the large particles, i.e., $a(\mathrm{LS}) \approx a(\mathrm{L})$. As can be seen in Fig. 8, a successful superposition of all observed modes in LS, L, and S is obtained in the presentation $\omega a/c$ versus qa with no adjustable parameter. Superposition of the dispersion curves in LS and the single crystalline components L and S in a $\omega R/c$ versus qR diagram is successfully obtained only if the effective radius $R(\mathrm{LS})$ in LS equals $R(\mathrm{L})$, the radius of the large particles. In this case, according to Table I, a/R is (almost) the same for the above three systems (of course, a/R is much different for the S particles of LS, but the effect of the eigenmodes of these particles on the dispersion diagram is marginal for reasons that will be explained below), and thus the $\omega R/c$ versus qR and the $\omega a/c$ versus qa diagrams are equivalent. As shown in the inset of Fig. 8, in the low-q region, the phonon

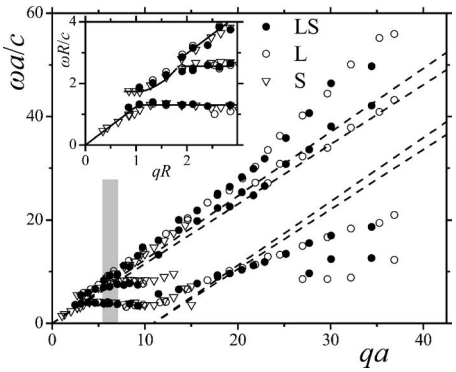

FIG. 8. A reduced phonon dispersion diagram for LS, L, and S, using the experimental points of Figs. 5 and 6, the relevant dimensions from Table I, and the (longitudinal) sound velocity c in the solvent. The notation is as in Fig. 5. The inset shows a detailed view of the corresponding $\omega R/c$ vs qR dispersion diagram about the hybridization gaps, with R being the particle radius (for LS, R is the radius of the L particles). The lines are a guide to the eye.

dispersion in the binary crystal LS is indistinguishable from those in the single crystalline components L and S. The effective-medium sound velocity in LS is by about 6% higher than that in L and S because of the larger fractional volume occupied by the particles (see Table I). However, the acoustic phonon of the average medium in the region $qR \leqslant 1$ is experimentally accessible only in the S system, and the above difference is not discernible in the figure.

The hybridization gap in the vicinity of the eigenfrequencies of particle modes is manifested in LS about the quadrupole mode of the large (L) *and not* of the small (S) particles. A rationalization of this finding stems from an inspection of the unit cell of the LS crystal in Fig. 1(a). In the NaCl-type crystalline arrangement of the L and S particles, the larger volume-filling fraction $[\phi(\mathrm{L})/\phi(\mathrm{S}) \sim 15]$ apparently facilitates the interaction between the relatively more extended band of quadrupole modes of the L particles and the acoustic band of the effective medium, thus leading to a clear hybridization gap. This interaction is progressively suppressed for higher multipole modes because of their stronger localization about the particles. On the other hand, the S particles, though the same in number as the L ones, interact very weakly because of the relatively large interparticle spacing and form a very narrow band of strongly localized modes, which is not clearly observed experimentally.

It is interesting to note that, in LS, the band of quadrupole modes of the L particles is also the lowest in frequency, which intersects first with the effective-medium band. However, in general, responsible for the dominant hybridization gap is not the *lowest in frequency* but the *most extended* band of particle modes. And this band, according to the well-known tight-binding model in solid state physics,[8] will be the band formed from the particle modes that interact more strongly. These are the lowest multipole (quadrupole) modes of those particles which are closer to each other, i.e., those which occupy the largest volume of the colloidal crystal. It becomes clear now why the choice $R=R(\mathrm{L})$ for LS in the reduced frequency $\omega R/c$ or, equivalently, the choice $\omega a/c$ as reduced frequency ensures the successful superposition of all the observable bands of particle modes and hybridization

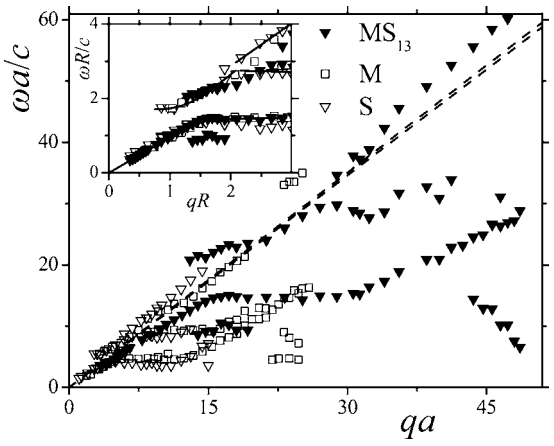

FIG. 9. A reduced phonon dispersion diagram for MS_{13}, M, and S using the experimental points of Figs. 5 and 6, the relevant dimensions from Table I and the (longitudinal) sound velocity c in the solvent. The notation is as in Fig. 5. The inset shows a detailed view of the corresponding $\omega R/c$ vs qR dispersion diagram about the hybridization gaps, with R being the particle radius (for MS_{13}, R is the radius of the S particles). The lines are guide to the eye.

gaps in the LS, L, and S systems. The relevant particle resonances occur at the same reduced frequencies and, moreover, the fractional volume occupied by the particles involved is not much different in all three systems (see Table I) implying interparticle interactions of comparable strength.

The Bragg modes, which are strong in crystalline structures are superimposed in all three systems in the presentation of Fig. 8. This is not surprising because the underlying Bravais lattice is the same (fcc) and the reduced wave number qa (or qR) is defined in terms of the appropriate lattice constant. In LS, the Bragg modes follow those of the L single crystal due to the similar a values.

The high-frequency modes that deviate from the effective-medium band in LS and L also show similar behaviors. This is in line with the interpretation of these modes as higher-order particle modes since, as explained above, the modes of the L particles in LS are more clearly manifested.

C. MS_{13} (cubic superlattice of $NaZn_{13}$ type)

In the MS_{13} system, the lattice spacing a assumes a quite different value in the mixed crystal and in the individual single colloidal crystals M and S. Due to this disparity, MS_{13} is suited for the differentiation between a hybridization and a Bragg phononic gap.[13] Superposition of the dispersion diagrams of the mixed MS_{13} crystal and the M and S crystals of the constituent particles in the low q region is successful only if the effective particle size of the binary MS_{13} crystal is set equal to R(S), the radius of the small particles, as shown in the inset to Fig. 9. If the lattice spacing a were chosen as the characteristic length, the superposition would fail as shown in the main plot of Fig. 9. Though in all three systems the effective-medium bands have almost the same slope (according to Table I the total fractional volume occupied by the particles is more or less the same in these three systems) and thus the corresponding points follow the same dispersion line, the position of the narrow bands of particle modes and the corresponding hybridization gaps is different. This was more or less expected from the large disparity of the ratio a/R for M, S, and the spheres of MS_{13} (see Table I). The particle resonances occur at the same reduced frequencies $\omega R/c$ but at very different reduced frequencies $\omega a/c$.

In MS_{13}, responsible for the dominant hybridization gap is the band of quadrupole modes of the small (S) and not of the large (M) particles. The flatband which originates from the quadrupole modes of the large particles, though the lowest in frequency, does not interact appreciably with the acoustic band of the effective medium, as can be seen in the lower panel of Fig. 6. This is the opposite situation of that in the LS system, where the large particles control the hybridization gap and can be easily understood. An inspection of the MS_{13} structure in Fig. 1(d), reveals that the closest proximity is that between the S particles in an icosahedral arrangement in the subcell, while the M particles are quite far from each other. In addition, the S particles are in majority with $\phi(\mathrm{S})/\phi(\mathrm{M}) \sim 2.5$.

The superposition of the Bragg modes in the mixed MS_{13} and the individual single colloidal crystals M and S is not only a matter of choice of the effective a in MS_{13}, i.e., the subcell ($a=710$ nm) versus the primitive unit cell ($a=1420$ nm), shown in Fig. 1(d). In this case, the Bravais lattices of MS_{13} (simple cubic) and M and S (both fcc) are different. Therefore the reciprocal lattice points (and consequently the Bragg modes) cannot be superimposed.

V. CONCLUDING REMARKS

Binary mixtures of monodisperse hard sphere colloids may self-assemble to form binary crystals similar to those encountered in atomic systems. The phonon propagation with wave number q was investigated in the case of two such polycrystalline suspensions at hypersonic frequencies f. The first binary system is a NaCl (fcc) crystal, which has a stoichiometry of LS and consists of large (L) particles with a radius $R=344$ nm arranged in a fcc lattice containing small particles (S) with a radius of 140 nm in the octahedral interstitial holes [Fig. 1(a)]. The second binary system is a MS_{13} superlattice structure made up of large (M) particles with $R=241$ nm and small (S) particles with a radius of 140 nm. In this structure the large spheres form a cube inside of which sit 13 small spheres, arranged at the 12 vertices and the center of an icosahedron. The lattice constants (a) of the mixed crystal LS and the single crystal L of the large particles are very close. Alternatively, the characteristic feature of the MS_{13} system is its large spacing which is distinctly different from the lattice parameter in the individual M and S crystalline components, i.e., $a(\mathrm{MS}_{13})a(\mathrm{M}) > a(\mathrm{S})$.

For both binary crystals, it is clearly demonstrated that the acoustic behavior is determined by the reduced quantity qR (insets of Figs. 8 and 9) and not qa (main plot of Fig. 9). However, the effective R is either that of the large particles (in LS) or that of the small particles (in MS_{13}). It is the same R that determines the eigenfrequency of the quadrupole particle modes responsible for the gap. The $\omega R/c$ versus qR scaling seems to work only in the low-q/low-f region and for the specific systems under consideration. This pertinent finding can be rationalized as follows: In this region, only the

effective-medium band interacts with the dominant bands of particle modes. The slope of the effective-medium band is nearly the same for all systems if their (total) volume-filling fractions are not very different. The position of the particle modes in $\omega R/c$ units is also the same. On the other hand, if in a binary system the volume-filling fractions of the constituent particles are very different, only the modes of the particles that occupy the largest volume dominate the dispersion relation. Choosing the radius of these particles in the $\omega R/c$ versus qR plot, the position of the relevant particle modes in $\omega R/c$ units is the same. Moreover, the hybridization strength is very similar at comparable volume-filling fractions of the relevant particles irrespective of their size.

A desirable universal dispersion diagram encompassing the present findings for the phonon propagation in mixed colloidal crystals, even if they are made of the same materials cannot be easily constructed. It is not evident that such a diagram can encompass different particle concentrations and structural characteristics. For instance, particle concentrations influence, besides the effective-medium behavior, the size of the hybridization gaps. At relatively large volume fraction ϕ (0.418, 0.545, 0.670) one clearly observes bands of quadrupole (and octapole) particle modes as well as the corresponding hybridization gaps. At $\phi=0.174$ one can see a flatband of quadrupole particle modes but not a hybridization gap. Finally, at $\phi=0.045$, even the flatband of quadrupole particle modes is hardly discernible. On the other hand, the structural arrangement is crucial for the Bragg-type modes. The degree of order is also an issue. For all the above reasons, a universal dispersion diagram and general conclusions, deduced from results on a restricted number of specific systems, might be misleading and missing their purpose.

Finally, it should be noted that, while for the occurrence of the phononic hybridization gap [resulting from the interaction of the lowest ($l=2$) particle modes with the acoustic modes of the average medium] crystalline order is not a prerequisite, the formation of a Bragg gap (occurring at the boundaries of the first BZ) requires single crystalline structures. For hypersonic gaps, fabrication at the submicron scale is necessary, using state-of-the-art techniques such as self assembly[3] and holographic interference lithography.[20] Besides the fundamental research interest in phononic crystals in general, hypersonic crystals hold promise for new potential applications.[21]

ACKNOWLEDGMENTS

Partial financial support of the EU through the Network of Excellence SoftComp (NMP3-CT-2004-502235) is gratefully appreciated.

[1] P. N. Pusey, in *Liquids, Freezing and the Glass Transition*, edited by J. P. Hansen, D. Levesque, and J. Zinn-Justin (Elsevier, Amsterdam, 1991).
[2] J. D. Joannopoulos, R. D. Meade, and J. N. Winn, *Photonic Crystals: Molding the Flow of Light* (Princeton University Press, Princeton, 1995).
[3] W. Cheng, J. J. Wang, U. Jonas, G. Fytas, and N. Stefanou, Nat. Mater. **5**, 830 (2006).
[4] J. Liu, L. Ye, D. Weitz, and P. Sheng, Phys. Rev. Lett. **65**, 2602 (1990); L. Ye, J. Liu, P. Sheng, and D. Weitz, Phys. Rev. E **48**, 2805 (1993).
[5] D. O. Riese and G. H. Wegdam, Phys. Rev. Lett. **82**, 1676 (1999).
[6] R. S. Penciu, G. Fytas, E. N. Economou, W. Steffen, and S. N. Yannopoulos, Phys. Rev. Lett. **85**, 4622 (2000).
[7] R. S. Penciu, H. Kriegs, G. Petekidis, G. Fytas, and E. N. Economou, J. Chem. Phys. **118**, 5224 (2003).
[8] N. W. Ashcroft and N. D. Mermin, *Solid State Physics* (Saunders College, New York, 1976).
[9] M. H. Kuok, H. S. Lim, S. C. Ng, N. N. Liu, and Z. K. Wang, Phys. Rev. Lett. **90**, 255502 (2003); **91**, 149901(E) (2003).
[10] W. Cheng, J. J. Wang, U. Jonas, W. Steffen, G. Fytas, R. S. Penciu, and E. N. Economou, J. Chem. Phys. **123**, 121104 (2005).
[11] A. Urbas, E. L. Thomas, H. Kriegs, G. Fytas, R. S. Penciu, and E. N. Economou, Phys. Rev. Lett. **90**, 108302 (2003).
[12] H. Kriegs, G. Petekidis, G. Fytas, R. Penciu, E. N. Economou, and A. B. Schoefield, J. Chem. Phys. **121**, 7849 (2004).
[13] I. E. Psarobas, A. Modinos, R. Sainidou, and N. Stefanou, Phys. Rev. B **65**, 064307 (2002).
[14] M. Sigalas and E. N. Economou, Solid State Commun. **86**, 141 (1993).
[15] M. S. Kushwaha, P. Halevi, L. Dobrzynski, and B. Djafari-Rouhani, Phys. Rev. Lett. **71**, 2022 (1993).
[16] Z. Liu, X. Zhang, Y. Mao, Y. Y. Zhu, Z. Yang, C. T. Chang, and P. Sheng, Science **289**, 1734 (2000).
[17] J. V. Sanders, Philos. Mag. A **42**, 705 (1980); M. J. Murray and J. V. Sanders, *ibid.* **42**, 721 (1980).
[18] P. Bartlett, R. H. Ottewill, and P. N. Pusey, Phys. Rev. Lett. **68**, 3801 (1992); N. Hunt, R. Jardine, and P. Bartlett, Phys. Rev. E **62**, 900 (2000); A. B. Schofield, *ibid.* **64**, 051403 (2001); A. B. Schofield, P. N. Pusey, and P. Radcliffe, *ibid.* **72**, 031207 (2005).
[19] G. C. Gaunaurd and W. Wertman, J. Acoust. Soc. Am. **85**, 541 (1989).
[20] T. P. Gorishnyy, C. K. Ullal, M. Maldovan, G. Fytas, and E. L. Thomas, Phys. Rev. Lett. **94**, 115501 (2005).
[21] T. P. Gorishnyy, C. K. Ullal, M. Maldovan, and E. L. Thomas, Phys. World **18**, 24 (2005).